Relative velocity fluctuations in turbulent flows at moderate Reynolds numbers. I. Experimental

P. Tong and W. I. Goldburg
Department of Physics and Astronomy, University of Pittsburgh, Pittsburgh, Pennsylvania 15260

(Received 15 January 1988; accepted 24 June 1988)

Turbulent pipe flow and grid flow have been explored by the scattering of light from small particles suspended in a fluid. Laser Doppler velocimetry and visual observation were used to characterize the gross features of the flows. However, novel information came from the homodyne correlation function $g(t)$, which was measured as a function of the Reynolds number, the photon momentum transfer, and the size of the scattering volume. In terms of these control variables, $g(t)$ was found to be of scaling form. Using such measurements one can deduce from the probability distribution function, $P(V,R)$, that two particles, separated by a distance R, have velocity *difference* $V(R,t)$. For small-velocity fluctuations, the scaling behavior of $g(t)$ implies that $P(V,R)$ has the form $Q[V/\bar{u}(R)]/\bar{u}(R)$. This self-similarity in $P(V,R)$ is seen only when Re exceeds a transition Reynolds number Re_c. The measured scaling velocity $\bar{u}(R)$ has the form $\bar{u}(R) \sim R^{\zeta}$, with ζ increasing from 0 at $\mathrm{Re} = \mathrm{Re}_c$ to $\sim \frac{1}{3}$ at the maximum attainable levels of turbulence. This scaling behavior was seen in both the grid and pipe flows. By measuring $g(t)$ at very small t, one can also obtain information about the large-velocity fluctuations. It is found that $P(V,R)$ is well approximated by the product of a Lorentzian and a Gaussian function with characteristic velocities $\bar{u}(R)$ and $u(R)$, respectively. Here $u(R)$ identifies the large-velocity fluctuations.

I. INTRODUCTION

Turbulence is generally viewed as a cascade of energy, injected at a large spatial scale, to smaller and smaller eddy sizes.[1] Of special interest is the velocity difference $\mathbf{V}(R,t)$ associated with eddies of size R. If follows from the eddy cascade picture that these velocity fluctuations are self-similar at various spatial scales R in the inertial range, where the energy cascade proceeds without dissipation. This implies[2] that the moments of $\mathbf{V}(R,t)$, $\langle|\mathbf{V}(R,t)|^n\rangle$, vary as some power of R. More generally, the probability distribution function $P(\mathbf{V},R)$ of $\mathbf{V}(R,t)$ is a homogeneous function, $Q[|\mathbf{V}|/u(R)]/u(R)$, where $u(R)$ is a characteristic velocity.[3] The self-similarity, or scaling, is generally thought to hold only at extremely large Reynolds number, where many experiments have been carried out.[4,5] There has also developed in recent years a great interest in hydrodynamic flows in the opposite regime of low Reynolds number at the onset of turbulence.[6,7] The experiment described here is a light scattering study of turbulent flows at intermediate Reynolds number, where self-similarity is also seen.

It was shown[8–10] that the distribution function $P(\mathbf{V},R)$ is accessible by the technique of photon correlation homodyne spectroscopy (HS).[11] This was first demonstrated many years ago by Bourke *et al.*[10] The photon correlation technique used here differs from the standard one of laser Doppler velocimetry (LDV),[12,13] in that LDV measures the local velocity $\mathbf{v}(r(t))$, whereas homodyne spectroscopy senses the instantaneous velocity difference $\mathbf{V}(R,t)$. With the HS scheme the scattering is produced by small seed particles in the fluid, which follow the local flow. The photodetector records the scattered light, which is the beating of Doppler-shifted light scattered by pairs of flowing particles. The output of the detector is therefore modulated at a frequency equal to the difference in Doppler shifts of all particle pairs in the scattering volume. For each particle pair, separated by a distance R, this difference is

$$\mathbf{q}\cdot[\mathbf{v}(r(t)) - \mathbf{v}(r(t) + R)] = \mathbf{q}\cdot\mathbf{V}(R,t),$$

where the scattering vector $\mathbf{q}$ has the amplitude

$$q = (4\pi n/\lambda)\sin(\theta/2).$$

Here θ is the scattering angle, n the refractive index of the fluid, and λ is the wavelength of the incident light. With this so-called homodyne method, one records the intensity correlation function $g(t) = \langle I(t')I(t'+t)\rangle/\langle I(t')\rangle^2$, where $I(t)$ is the intensity of scattered light, and the angle brackets represent an ensemble average over many realizations.

The correlation function $g(t)$ has the following form[8,9]:

$$g(t) = 1 + G(qt,L), \tag{1}$$

where

$$G(qt,L) = \int_0^L dR\, h(R) \int_{-\infty}^{\infty} dV\, P(V,R)\cos(qtV). \tag{2}$$

In the above, V is the component of $\mathbf{V}(R,t)$ along the scattering vector $\mathbf{q}$, and $h(R) = 2(1 - R/L)/L$ is the number fraction of particle pairs separated by a distance R in the scattering volume. The scattering volume viewed by a photodetector is assumed to be quasi-one-dimensional with length L. Equations (1) and (2) indicate that the light scattered by each pair of particles contributes a phase factor $\cos(qtV)$ (as a result of frequency beating) to the intensity correlation function $g(t)$, and $g(t)$ is an incoherent sum of these ensemble averaged (or time averaged) phase factors

 0031-9171/88/102841-08$01.90

over all the particle pairs in the scattering volume. The ensemble average of the phase factor, $\cos[\mathbf{q}\cdot\mathbf{V}(R)t]$, involves the velocity distribution function $P(V,R)$. The weighted average over R is required because the detector is sensitive to all particle pairs in the scattering volume, and for small R, more pairs will be found in the scattering volume than that for larger R.

When the distribution function $P(V,R)$ has the scaling form $Q(V/u(R))/u(R)$ as mentioned above, Eq. (2) becomes

$$G(qt,L) = \int_0^L dR\, h(R) F(qtu(R)), \tag{3}$$

where $F(x)$ is the Fourier cosine transform of $Q(V/u(R))$. The above calculation was made by assuming that $g(t)$ varies on only one dominant time scale. This assumption is valid in our experiment where the time scale of interest is much shorter than other characteristic times associated with the decay of $g(t)$. These characteristic times are the turbulent turnover time, the time associated with the particle diffusion, and the transit time caused by the passage of particles through a laser beam of small diameter.[8] The HS technique yields information about velocity fluctuations without introducing an invasive probe, such as a hot wire anemometer.[14] Nor is it necessary to invoke Taylor's "frozen turbulence" assumption[15] to interpret the measurements.

Recently, the present authors and their collaborators have exploited the HS technique to study turbulent pipe flow behind a grid at moderate Reynolds numbers.[8] The Reynolds number of this grid flow is defined as $\mathrm{Re} = UM/\nu$, where U is the mean flow velocity at the centerline of the pipe, M (= 3.1 mm) is the aperture size of the grid that generates turbulence, and ν is the kinematic viscosity of the fluid. It was found that when Re becomes larger than a transition Reynolds number, Re_c (~300–400 for the grid flow), the function $G(qt,L)$ extracted from the measured $g(t)$ has the scaling form

$$G(qt,L) = G(\kappa), \tag{4}$$

where $\kappa = qt\bar{u}(L)$. Here $\bar{u}(L)$ is the characteristic turbulent velocity at length scale L. Both the functional form of $G(\kappa)$ and its scaling argument κ provide information about the statistical properties of the velocity fluctuations $V(R,t)$. Measurements of $g(t)$ suggest that the distribution function $P(V,R)$ for small values of $V(R,t)$ is Lorentzian-like when $\mathrm{Re} \gtrsim \mathrm{Re}_c$. Equivalently the characteristic function $F(x)$ [the Fourier transform of $P(V,R)$] in Eq. (3) decays exponentially. We also found that the characteristic velocity $\bar{u}(L)$ has a scaling form $\bar{u}(L) \sim L^{\zeta}$. The exponent ζ shows a nontrivial Re dependence and reveals a transitional character when Re is near and above Re_c. When $\mathrm{Re} \gtrsim 1400$, ζ has climbed to, and saturated at, a value close to $\frac{1}{3}$ (the Kolmogorov value).

In this paper we report a further HS study of turbulent grid flow, as well as pipe flow. The Reynolds number of the pipe flow is defined as $\mathrm{Re} = Ud/\nu$, where d (= 4.4 cm) is the diameter of the pipe. When Re becomes larger than Re_c (~3000–4000 for the pipe flow), the self-similar feature of the relative velocity fluctuations seen in the grid flow are also observed in pipe flow. When the Reynolds number is near and above Re_c, the scaling exponent ζ of the characteristic velocity $\bar{u}(L)$ has the form $\zeta(\mathrm{Re}) \sim [(\mathrm{Re} - \mathrm{Re}_c)/\mathrm{Re}_c]^{\phi}$ for both flows. We found that the distribution function $P(V,R)$ is well approximated by a product of a Lorentzian function and a Gaussian-like function. While the small-scale statistics of velocity fluctuations in pipe flow are similar to that of grid flow, there are some differences regarding the different geometries of the two flows.

In a future paper (denoted as II), we present a phenomenological model in an attempt to intercept our measurements. Using multifractal ideas,[16,17] we generalize the random beta model[18] to explore the Re dependence of the self-similarity of turbulence at moderate Reynolds number. According to this model, the scaling behavior of small-velocity fluctuations can be characterized by a single Re-dependent scaling exponent α_0. The calculated Re dependence of α_0 is consistent with the experiment described here.

Section II contains the experimental details, including a brief description of the experimental methods for visual observation of flows and laser Doppler velocimetry. The results appear in Sec. III, and the work is summarized in Sec. IV.

II. APPARATUS AND METHOD

The physical arrangement for the correlation function measurement is the same as that of Ref. 8 and is shown in Fig. 1(a). The water, seeded with polystyrene spheres of diameter 0.06 μm, is circulated through a closed system by a pump. Since the size of the polystyrene spheres is much smaller than the wavelength of the incident light ($\lambda = 0.488$ μm), the scattering by these particles is nearly isotropic. A section of the pipe (diameter = 4.4 cm) is made of glass to admit the incident laser beam and observe the scattering. Undesirable velocity fluctuations produced by the pump or by the pipe corners are damped out by a screen (SC) (aperture size = 2.0 mm) on the high-pressure side of the grid (G), which generated the turbulence. The aperture size of the grid, M, was 3.1 mm and the diameter of rods with which the grid is made was 1.5 mm. The measuring point was on the axis of the pipe and 28 cm downstream from the grid ($x/M = 90$). In the pipe flow experiment we simply removed both the grid and the screen. The temperature of the circulating water was stabilized at room temperature. The mean flow velocity U was varied by changing the pump speed.

Measurements of the correlation function $g(t)$ were performed using a standard light scattering apparatus and a multichannel correlator (Langley Ford 1096). The lens L_1 in Fig. 1(a) focuses the laser beam from an argon-ion laser to make the scattering volume as one dimensional as possible on the axis of the pipe (the focused beam diameter $\simeq 0.1$ mm), while L_2 forms an image of this volume on the slit S of that the size of the scattering beam is the same as that of its image (the magnification is 1). It is the light passing through the slit that illuminates the photomultiplier (PM) located far behind the slit. The water inlet and outlet as well as a standpipe (BT), where air bubbles can leave the fluid, are also shown in Fig. 1(a). The incident beam direction and the

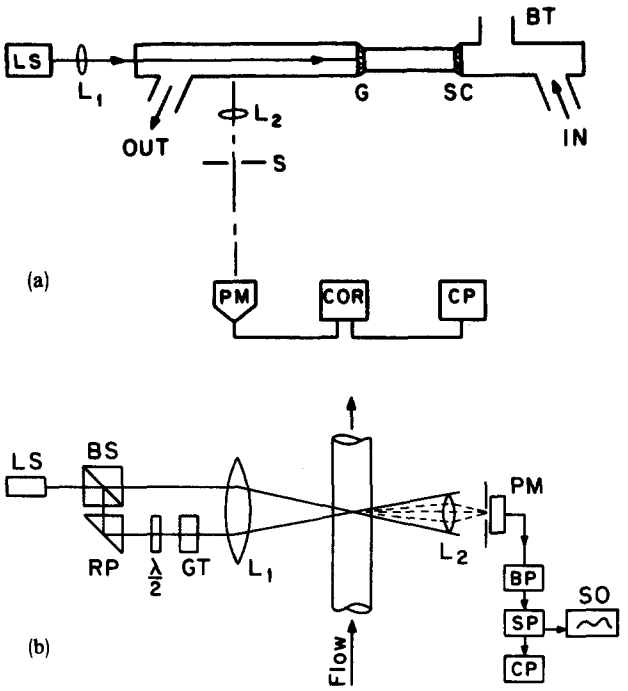

FIG. 1. Schematic diagram of (a) homodyne spectroscopy setup: LS, argon ion laser; L_1 and L_2, lenses; S, slit; G, grid; SC, screen; BT, air bubble trap; PM, photomultiplier; COR, correlator; CP, computer; IN, inlet of flow; OUT, outlet of flow; and LDV setup: LS, He–Ne laser; BS, beam splitter, RP, right-angle prism; $\lambda/2$, half-wave plate; GT, Glan–Thompson polarizer; L_1, L_2, lenses; PM, photomultiplier; BP, bandpass filter; SP, signal processor; SO, storage oscilloscope; CP, computer.

aligned optical apparatus (the lens L_2, the slit S, and the photomultiplier PM) define the scattering angle θ. The output signal from the photomultiplier was converted into pulses of standard size, which went to the correlator (COR), whose output gives the correlation function $g(t)$. Also indicated is the computer (CP) (PDP-11/24) for storing and analyzing the data.

In order to classify the pipe flow and the grid flow, two kinds of ancillary measurements were carried out, namely, visual observation of the flow and laser Doppler velocimetry (LDV).[12,13] To view the flow, the incident laser beam from an argon-ion laser entered the fluid along the axis of the pipe and was defocused by a lens. The laser beam then illuminated the large center region of the pipe. The circulating fluid in the pipe was tap water, and the moving traces of big dust particles in the water could be seen by eye.

The dual-beam forward-scattering method[12] was used in measuring the longitudinal local velocity $v(r(t))$. The optical layout of the laser Doppler velocimeter is shown in Fig. 1(b). The cubic beam splitter (BS) and the right-angle prism (RP) produce two parallel beams. The right-angle prism sits on an optical mount that has fine orientational controls to bring the two beams into exact parallelism. The half-wave plate ($\lambda/2$) and the Glan–Thompson polarizer (GT) are adjusted so that the two beams have the same intensity and the same polarization. The lens L_1 with a focal length of 12 cm focuses the interfering beams at the point where the velocity is to be measured. The lens L_2 collects the scattered light, whose amplitude is modulated as particles pass through the fringes produced by the interfering beams. The modulated light is focused on the photomultiplier (PM). The LDV system was mounted on a train so that it could be easily calibrated and could be moved without realignment to obtain velocities at different points in the flow.

The photomultiplier was operated in the current mode to detect the Doppler signal at a frequency of the order of 100 kHz. The photomultiplier output was first filtered by a bandpass filter (BP), and then went to a TSI Model 1980 counter-type signal processor (SP). The counter was operated so that it counted no less than 16 cycles of a Doppler burst, and rejected the signal if the cycle period within each burst fluctuated by more than 1%. The seed particles were polystyrene spheres of 1 μm in diameter. The mean velocity, the variance of the local velocity, and the local velocity distribution can be deduced from an ensemble of velocity measurements that were stored in the computer (CP). The typical sampling rate in the LDV measurements was about 1 Hz. Both the fast digital oscilloscope (SO) display of individual Doppler bursts and the measurements of the velocity distributions showed that our velocity measurements were very accurate.

III. EXPERIMENTAL RESULTS

A. Visual observation of flows and LDV measurements

Before turning to the discussion of our new findings obtained from the measurements of the intensity correlation function, we first discuss results from the visual observation of flows and from the LDV measurements. The main aim of these ancillary observations was to establish that the turbulence in our system (both the grid flow and the pipe flow) was typical of previously studied flows of the same geometry.[19–21] The reader who wants to learn first about our new results should turn to Secs. III B and III C.

As shown in Fig. 2, the normalized mean velocity profile of the grid flow in the direction transverse to the mean flow direction becomes flat rather than parabolic when the Reynolds number is above 280. The velocity was measured 28 cm downstream from the grid ($x/M = 90$), the same position at which HS measurements were carried out. The flat velocity profile indicates the onset of turbulent flow. Similar flatten-

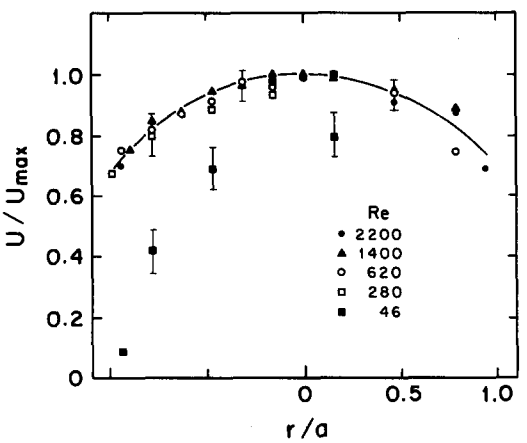

FIG. 2. The normalized mean velocity profiles in the transverse direction for grid flow at indicated Reynolds numbers. Here U_{max} is the mean velocity at the centerline of the pipe, and a is the radius of the pipe.

ing of the mean velocity profile in the pipe flow was also observed when Re becomes larger than the transition Reynolds number of the pipe flow.

A Gaussian-like local velocity probability distribution was observed in our flows. An example of the distribution function is displayed in Fig. 3, which shows the local velocity distribution function of pipe flow at Re = 20 000. The horizontal axis in the plot is the Doppler frequency, which is proportional to the local velocity of fluid. The bandwidth in the measurement, 50–120 kHz, was set by the bandpass filter. We repeatedly measured the local velocities (3000–1000 data points for each record) for various mean flow speeds at six downstream positions. Both the grid flow and the pipe flow show similar behavior of the velocity distributions at different downstream positions and different Reynolds numbers. These velocity distributions are Gaussian-like with a kurtosis (the fourth moment normalized by the square of the variance) close to 3 and a small skewness (the third moment normalized by the variance to the $\frac{3}{2}$ power). It should be noted that, due to the intrinsic limitation of the LDV technique and the slow sampling rate in our measurements (as a result of the severe conditional sampling and sparse seeding), our LDV measurements were insensitive to rare but large relative velocity fluctuations even though they were very noticeable by visual observation.

Comparing the grid and pipe flows, the LDV measurements reveal that the turbulent intensity near the pipe wall in the pipe flow is much larger than that in the grid flow at equal values of U. The turbulent intensity is defined as $\sqrt{\langle(\delta v)^2\rangle}/U$, where δv is the fluctuating part of the flow velocity about its mean value U. This indicates that the pipe-generated turbulence is produced by the boundary and that the boundary effect on the grid flow is relatively small. The difference between the two flows becomes more apparent from the way that both flows change their character as Re is increased to the transition Reynolds number Re_c. This process was best followed by the visual observation of flows, which is also a useful way to study turbulence at low Reynolds numbers.

For the grid flow, when $\mathrm{Re} \lesssim 20$, which is far below Re_c ($\sim$300–400), the flow is seen to be laminar throughout the entire test section, which extended 30 cm downstream from the grid. The moving traces of particles are straight lines parallel to the axis of the pipe. As Re is increased to about 100, small-scale local velocity disturbances appear first near the grid. The trajectory of the individual particles becomes entangled in very small regions of size ~ 1 cm near the grid, and they are almost straight lines farther downstream. This suggests that these local disturbances (eddies) are generated by the grid. The number of visible eddies at this stage is quite small. At this Reynolds number we also observed that in the "eddy region," the velocity fluctuation $V(R,t)$ is larger than the mean flow velocity U, and in the "laminar"-like region the velocity fluctuations are small compared to U. When $\mathrm{Re} \sim 200$, the apparent number of eddies is increased and eddies near the grid form a turbulent region, within which the particle trajectories become intertwined. As Re is increased toward Re_c, the "laminar"-like region progressively decreases in volume, and the turbulent region expands in the downstream direction. Finally, when $\mathrm{Re} \gtrsim \mathrm{Re}_c$ the turbulent region occupies the entire test section. Now the further development of the turbulent flow becomes hard to follow by eye. We have found that the parameter Re_c can also be deduced from the measurements of $g(t)$.[8,9] One purpose of our visual observations was to see if the flow pattern changes as $\mathrm{Re} = \mathrm{Re}_c$ is crossed.

For the pipe flow, when $\mathrm{Re} \lesssim 450$, the flow is laminar in the entire test section and the traces of particles are straight lines parallel to the axis of the pipe. As Re is increased to ~ 1600, particles in the flow start to meander slowly in both the longitudinal and transverse directions. When Re reaches ~ 2000, eddies appear first in the downstream region of the test section. As Re approaches Re_c ($\mathrm{Re}_c \sim 3000$–4000), the turbulent region expands in the upstream direction, a behavior opposite to that of the grid flow. Occasionally, eddies were seen to sweep through the illuminated region from the pipe wall. When $\mathrm{Re} \sim \mathrm{Re}_c$, the turbulent region occupies the entire test section as in the grid-generated turbulence. We emphasize that the transition from laminar to turbulent flow occurs at approximately the same velocity for both pipe and grid flows, even though the Reynolds numbers are very different.

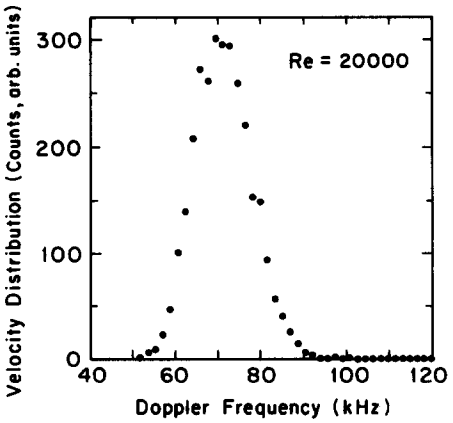

FIG. 3. The local velocity distribution of pipe flow at Re = 20 000.

B. Small relative velocity fluctuations

As discussed in Sec. I, the function $G(qt,L)$ extracted from the measured $g(t)$ in the grid flow has the scaling form $G(\kappa)$ in Eq. (4). The data analysis[8] suggests that for small relative velocity fluctuations, $P(V,R)$ is Lorentzian-like, for which moments higher than the first diverge. Of course $P(V,R)$ cannot remain Lorentzian for very large velocity fluctuations, since the turbulent energy injection rate is finite. Referring to the above experimental results, Onuki proposed[22] that the three-dimensional distribution $P(\mathbf{V},R)$ for the isotropic turbulent flow is a product of two functions. One function is associated with the small-velocity fluctuations, having the Lorentzian-square form (in the three-dimensional case) and being characterized by a scaling velocity $\bar{u}(R)$ as mentioned above. The other function is associated with the large-velocity fluctuations, having finite

moments and being characterized by a "cutoff" velocity $u(R) \gg \bar{u}(R)$. Under the assumption that the moments $\langle |\mathbf{V}(R,t)|^n \rangle$ obey the original Kolmogorov theory,[1] it is shown by Onuki that the two characteristic velocities $\bar{u}(R)$ and $u(R)$ have the same R dependence [$\bar{u}(R) \sim u(R) \sim R^{1/3}$]. Onuki also predicts that the characteristic function F in Eq. (3) should cross over from exponential-like form [$F \sim 1 - \bar{u}(R)qt$] to Gaussian-like form [$F \sim 1 - \text{const}\, u(R)\bar{u}(R)(qt)^2$] when $qtu(R) \sim 1$.

We first discuss here the long-time [$qtu(L) \gg 1$] behavior of the correlation function $g(t)$ in the pipe flow. These measurements provide information about the small-scale statistics of the small relative velocity fluctuations [since $V(R,t)/u(R)$ and $qtu(R)$ are two conjugate variables in the Fourier transformation, $qtu(R) \gg 1$ means $V(R,t)/u(R) \ll 1$]. In Sec. III C we will discuss the statistical properties of large-velocity fluctuations [$V(R,t)/u(R) \sim 1$], in which case the correlation function $g(t)$ is measured at very small times so that $qtu(L) \sim 1$.

It is found that the measured $G(qt,L)$ in pipe flow (grid removed) has the same self-similar feature as that of the grid flow, the functional form of $G(qt,L)$ in the pipe flow being the same as that shown in Eq. (4). In Ref. 8 we detailed the procedure with which it was established that $G(qt,L)$ has the scaling form $G(\kappa)$. The scaling result, $G(qt,L) = G(qt\bar{u}(L))$, where $\bar{u}(L) \sim L^{\zeta}$, implies that log–log plots of $G(qt,L)$ at various values of q and L can be brought into coincidence by sliding them horizontally with respect to each other. The same scaling feature is also found in pipe flow when Re exceeds some particular value, i.e., Re_c. In grid flow $\mathrm{Re}_c \sim 300$–400, and in the pipe flow $\mathrm{Re}_c \sim 3000$–4000. Figure 4 shows $G(\kappa)$ as a function of κ defined in Eq. (4) for various values of Re, slit width L, and scattering angle θ. It is seen that the functional form of $G(qt,L)$ in the two flows is the same. However, the absolute value of the decay time, $T(L) \sim [q\bar{u}(L)]^{-1}$, of $G(\kappa)$ is different in the two flows, though the L dependence of $T(L)$ is the same. In fact, we observed that under the same physical conditions, the correlation function $g(t)$ in pipe flow decays faster than that in grid flow. This difference in decay time was found to be independent of the size of the scattering volume L when q and Re were fixed. This is related to the fact that the two flows may have different proportionality constants in the equation $T(L) \sim [q\bar{u}(L)]^{-1}$.

The L dependence of the characteristic velocity $\bar{u}(L)$ in pipe flow is found by measuring the decay time $T(L)$ of $G(qt,L)$. The integral in Eq. (3) can be approximated by a sum $\Sigma_{n=0}^{N} A_n F(x_n)$, where the $N+1$ weights A_n and the $N+1$ abscissas x_n are determined using the Gaussian quadrature method.[23] The error introduced by this approximation is estimated in terms of the $(2N+2)$-th derivative of $F(x)$.[23] In particular, we found that $G(qt,L)$ in Eq. (3) can be approximated by the characteristic function $F(x)$ evaluated at its zeroth-order abscissa $0.643qt\bar{u}(L)$. It turns out that the error introduced by this approximation is no more than 4% when $qt\bar{u}(R) \leqslant 1$. Hence $G(qt,L)$ extracted from the measured $g(t)$ at small t is proportional to the characteristic function $F(0.643qt\bar{u}(L))$. Figure 5 is a semilog plot of $G(qt,L)$ versus time t at $\mathrm{Re} = 23\,000$, $\theta = 90°$, and $L = 0.3$ mm. When $t \lesssim 20\,\mu$sec, $\log[G(qt,L)]$ is a linear function of t, which indicates that the characteristic function $F(x)$ decays exponentially. The slope of the straight line (see Fig. 5) yields a characteristic decay rate, $1/T(L)$, of $G(qt,L)$. From a series of such plots, corresponding to various L but fixed q, we found that T as a function of L obeys a power law, $T(L) \sim L^{-\zeta}$, as is seen in Fig. 6. Figure 6 shows log–log plots of the decay time T vs L. The three curves in the figure, all made at $\theta = 90°$, correspond to $\mathrm{Re} = 5400$, 14 300, and 26 000. The lower two curves of Fig. 6 show that $\log[T(L)]$ lies on a straight line when L is in the range $0.1\ \text{mm} \leq L \leq 1.0$ mm.

Experimentally we have verified that the power law behavior at large L was limited by the coherence length of the optical system.[11] The lower cutoff at small L was controlled by the diameter of the incident laser beam (~ 0.1 mm). When $L \lesssim 0.1$ mm, the measured decay time is determined by the width of the beam rather than its length, and a further decrease of L will not change T. From the straight line segment (solid line in Fig. 6) we can extract the slope ζ, which shows a Re-dependent feature. The number below each straight line in Fig. 6 is the value of ζ at the indicated Re. We speculate that T should be independent of L when L is less than the Kolmogorov dissipation length L_d, since there are no eddies smaller than this size. One may hope to measure L_d by finding the value of L at which T levels off as L is decreased. In fact, it can be seen from Fig. 6 that when $\mathrm{Re} = 5400$, T levels off at $L \simeq 0.3$ mm (dashed line), which

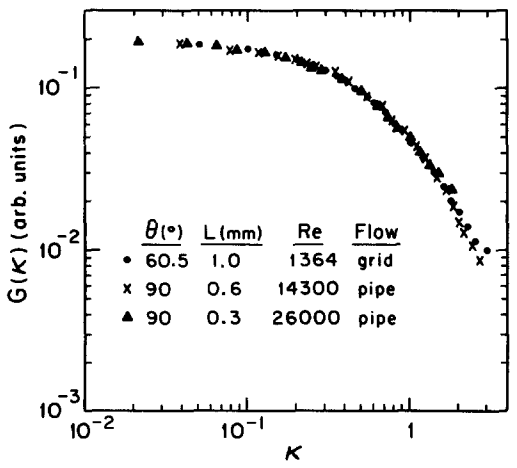

FIG. 4. The homogeneous function $G(\kappa)$ vs $\kappa = qt\bar{u}(L)$ for both pipe and grid flows at indicated parameters.

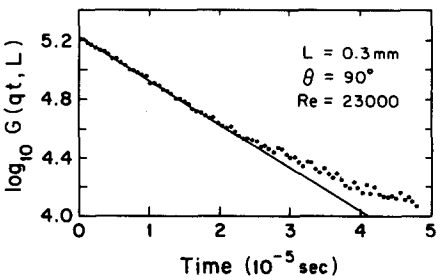

FIG. 5. A plot of $\log[G(qt,L)]$ vs t for pipe flow at indicated parameters.

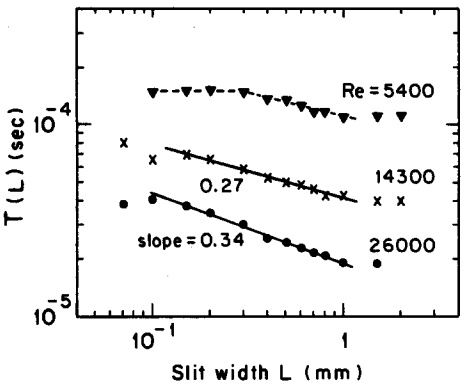

FIG. 6. The variation of the decay time T with L for pipe flow at different Re and fixed θ (90°). The number labeled below a line is the slope of that line.

suggests that $L_d \simeq 0.3$ mm at this turbulent level.

The Re dependence of the exponent ζ in pipe flow is displayed in Fig. 7. For the purpose of comparison we also include in the inset a plot of ζ vs Re in the grid flow.[8] The two curves are similar except that the two flows have a different transition Reynolds number, i.e., Re_c. For both flows ζ saturates at $\sim\frac{1}{3}$ (the Kolmogorov value) at higher Re, and there is a small amplitude oscillation superimposed on the saturation line of ζ. This oscillation may be real in spite of the large uncertainty.

In the grid flow we have found[8] that ζ as a function of Re near Re_c was well fitted to the equation

$$\zeta(\mathrm{Re}) = C\omega^{\phi}, \tag{5}$$

where $\omega = (\mathrm{Re} - \mathrm{Re}_c)/\mathrm{Re}_c$. Here C and ϕ are fitting parameters. The measured ζ in the pipe flow can also be fitted to Eq. (5). But this time the transition Reynolds number Re_c and the exponent ϕ are different. Because of the large uncertainty in Re_c, the exponent ϕ is not well determined. Our data were fitted to Eq. (5) with ϕ, Re_c, and C as fitting parameters. Figure 8 shows the fitting results for the data

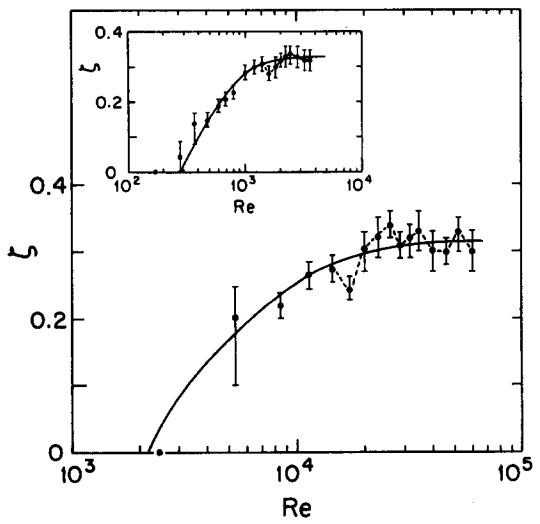

FIG. 7. The exponent ζ as a function of Re in pipe flow. The solid curve is drawn by eye through the data points, and the dashed curve shows the oscillatory behavior of ζ. The inset shows ζ vs Re in grid flow.

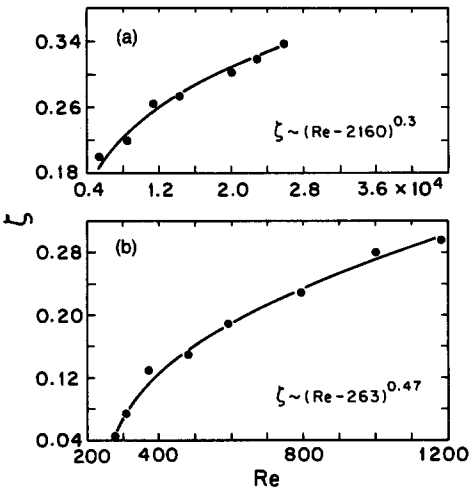

FIG. 8. The variation of ζ with Re near the transition Reynolds number Re_c. The solid curve is a fit to Eq. (5); (a) pipe flow, (b) grid flow.

from Fig. 7. For the pipe flow [upper curve (a)] the fitted results are $\mathrm{Re}_c = 2160 \pm 1000$ and $\phi = 0.30 \pm 0.1$. For the grid flow [lower curve (b)] $\mathrm{Re}_c = 263 \pm 6.4$ and $\phi = 0.47 \pm 0.05$. The large uncertainty of the fitting parameters in the pipe flow is due to the lack of data at small ω.

C. Large relative velocity fluctuations

As mentioned above, the functional form of the characteristic function F should cross over from exponential-like to Gaussian-like when $qtu(L) \sim 1$.[22] Hence if the sampling time of the correlator is set so small that $qtu(L) \sim 1$, the measured correlation function should change its functional form. In this section we discuss this short-time crossover of $g(t)$ in the grid flow.

If $P(V,R)$ is a product of two functions, the Fourier transform of $P(V,R)$ is the convolution of the two individual Fourier transforms. Because the distribution function $P(V,R)$ is assumed to have the form

$$P(V,R) \sim \exp(-\{v/[\sqrt{2}u(R)]\}^2)/\{1 + [V/\bar{u}(R)]^2\}, \tag{6}$$

the Fourier transform of $P(V,R)$ becomes

$$\begin{aligned} F(qt,R) &= \int_{-\infty}^{\infty} dt' \exp\left[-\left(\frac{(t'-t)}{a_3'}\right)^2\right] \\ &\quad \times \exp(-|t'|a_2') \\ &= a_1'\left[e^{-t/a_2'}\,\mathrm{erfc}\{-t/a_3' + a_3'/(2a_2')\}\right. \\ &\quad \left. + e^{t/a_2'}\,\mathrm{erfc}\{t/a_3' + a_3'/(2a_2')\}\right]. \end{aligned} \tag{7}$$

In the above, $\mathrm{erfc}\{x\}$ is the complementary error function, $a_2' = 1/[q\bar{u}(R)]$, and $a_3' = \sqrt{2}/[qu(R)]$. The parameter a_1' is an irrelevant constant. As mentioned in Sec. III B, with the Gaussian quadrature method[23] $G(qt,L)$ in Eq. (3) can be approximated by the characteristic function $F(x)$ evaluated at its zeroth-order abscissa $0.643x$. Therefore we have

$$\begin{aligned} G(qt,L) &\simeq a_1\{e^{-t/a_2}\,\mathrm{erfc}[-t/a_3 + a_3/(2a_2)] \\ &\quad + e^{t/a_2}\,\mathrm{erfc}[t/a_3 + a_3/(2a_2)]\}. \end{aligned} \tag{8}$$

where $a_2 = 1/[0.643\ q\bar{u}(L)]$, $a_3 = \sqrt{2}/[0.643qu(L)]$, and a_1 is also irrelevant. The error introduced by this approxima-

tion is no more than 13% when $qt\bar{u}(R) \leqslant 1$. Equation (8) was well fitted to the measured $G(qt,L)$ in the short-time region, where a_1, a_2, and a_3 are fitting parameters. A typical fit is displayed in Fig. 9 (solid line), which shows $G(qt,L)$ at $\mathrm{Re} \simeq 837$, $\theta = 90°$, and $L = 1.0$ mm. The fitting results are $a_2 = 4.77 \times 10^{-5}$ sec and $a_3 = 8.30 \times 10^{-6}$ sec.

The fitting results in Fig. 9 yield the ratio of the two decay times, $a_2/a_3 = 5.75$. Because the Gaussian factor in $P(V,R)$ introduces a roundoff to $G(qt,L)$ near $t = 0$, the absolute value of the slope of $G(qt,L)$ should decrease as t approaches zero. This decrease in slope is more clearly seen in the semilog plot of $G(qt,L)$ in the inset of Fig. 9. The inset of Fig. 9 also shows that $G(qt,L)$ at large t is best fitted to a single exponential, which is associated with the Lorentzian factor in $P(V,R)$. Many measured $G(qt,L)$ at various slit widths and Re were fitted to Eq. (8). It is found that the typical value of the ratio, $\gamma = u(L)/\bar{u}(L) = \sqrt{2}a_2/a_3$, is about 7, and does not change very much with Re and L. Using the fitted values of a_2 and a_3 we calculated that $u(L)/U \simeq 4.0\%$ and $\sqrt{\langle |\mathbf{V}|^2 \rangle}/U \simeq 2.7\%$, whereas the turbulent intensity measured by using LDV technique $\sqrt{\langle \delta v^2 \rangle}/U$ was about 5.6%.

Kraichnan pointed out[24] that the Brownian motion of the seed particles may affect the behavior of $G(qt,L)$ near $t = 0$. The effect of the Brownian motion is to contribute a factor $\exp(-2Dq^2t)$ to $G(qt,L)$, where D is the diffusion constant of Brownian particles. The diffusion time $T_D = (2Dq^2)^{-1}$ can be obtained by measuring the correlation function $g(t)$ when the flow is absent.[25] In our experiment the measured diffusion time $T_D = 1.13 \times 10^{-4}$ sec. By equating the Brownian motion contribution with that of the Gaussian roundoff of $G(qt,L)$ in the short-time region,[22] we can show that the Brownian motion will eventually dominate over the Gaussian roundoff effect when $t < 3\pi D/[u(L)\bar{u}(L)]$. This time is 6.83×10^{-6} sec for Fig. 9. The time resolution (the smallest sampling time) in the measurement of $G(qt,L)$ is 10^{-7} sec. Therefore the Brownian motion must be taken into account. The measured $G(qt,L)$ shown in Fig. 9 has been divided by $\exp(-t/T_D)$ to eliminate the Brownian motion effect. The Brownian motion effect can be neglected for flows at large Reynolds number.[26]

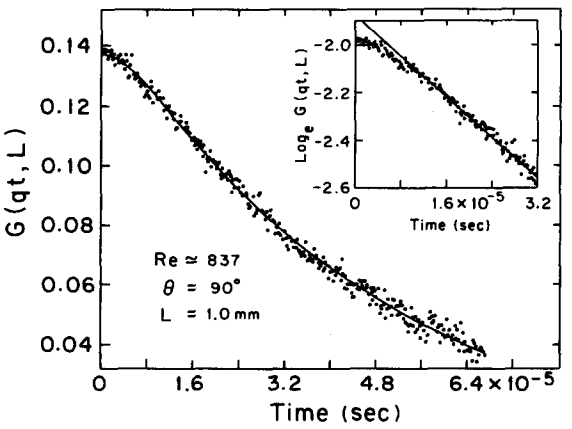

FIG. 9. A typical plot of the function $G(qt,L)$ vs t in grid flow. The solid curve is a fit to Eq. (8). The inset is a semilog plot of $G(qt,L)$ vs t at the same parameters. The solid line in the inset shows the limiting exponential behavior of $G(qt,L)$ when t is large. A small contribution to the decay from the Brownian motion of the seed particles has been divided out (see Sec. III C).

IV. SUMMARY

We have studied turbulent grid flow and pipe flow using the rarely exploited technique of photon correlation homodyne spectroscopy and other ancillary experimental techniques. Measurements of $g(t)$ give access to the relative velocity distribution function $P(V,R)$ that a pair of particles in the turbulent fluid, having separation R, *differ* in velocity by $V(R,t)$. The flow visualization and the LDV measurements as well as the HS measurements suggest that both the grid flow and the pipe flow change their character when the Reynolds number becomes larger than an experimentally determined transition Reynolds number, Re_c. In the grid flow $\mathrm{Re}_c \sim 300$–400, and in the pipe flow $\mathrm{Re}_c \sim 3000$–4000. When $\mathrm{Re} > \mathrm{Re}_c$, the distribution function $P(V,R)$ is well approximated by a product of a Lorentzian and a Gaussian-like function, and hence must be characterized by at least two parameters [$\bar{u}(R)$ and $u(R)$]. The scaling velocity $\bar{u}(R)$ characterizes the small velocity fluctuations while $u(R)$ identifies the large velocity fluctuations. This is in notable contrast to the local velocity distribution where a Gaussian-like probability distribution is obtained. Our finding that $P(V,R)$ is adequately represented by the product of Lorentzian and Gaussian factors is consistent with the notion that $V(R,t)$ arises from two distinct regions of the turbulent flow.[22]

It is found that the characteristic velocity $\bar{u}(R)$ has the scaling form $\bar{u}(R) \sim R^{\zeta}$. The exponent ζ shows a nontrivial Re dependence. In the vicinity of Re_c, ζ as a function of Re is approximately of the form $\zeta \sim [(\mathrm{Re} - \mathrm{Re}_c)/\mathrm{Re}_c]^{\phi}$. Near the maximum attainable values of Re, ζ has climbed to, and saturated at, the value close to $\frac{1}{3}$, i.e., the Kolmogorov value. Our measurements show that both the grid flow and the pipe flow possess the same self-similar feature, though there exist some differences between the two flows. The above described pilot experiment, carried out in the region of transition between laminar and turbulent flows, shows that the technique of photon correlation homodyne spectroscopy is a powerful tool for probing small-scale turbulent velocity fluctuations. It also shows that turbulent flows at even relatively low Reynolds numbers exhibit self-similarity that usually is associated only with flows at very high Reynolds numbers.

ACKNOWLEDGMENTS

We have benefited from illuminating discussions and correspondence with M. Nelkin, enjoyed a continuing fruitful interaction with A. Onuki, and are indebted to R. Kraichnan for his valuable suggestions and comments. We are grateful for the collaboration of A. Sirivat in the LDV measurements.

This work is supported by the National Science Foundation under Grant No. DMR-8611666.

[1] A. N. Kolmogorov, C. R. Dokl. Acad. Sci., URSS. **30**, 301; **31**, 538 (1941).
[2] U. Frisch, P. Sulem, and M. Nelkin, J. Fluid Mech. **87**, 719 (1978).

[3]C. W. Van Atta and J. Park, in *Statistical Models and Turbulence, Lecture Notes in Physics*, edited by M. Rosenblatt and C. W. Van Atta, (Springer, Berlin, 1972), Vol. 12, p. 402.
[4]F. Anselmet, Y. Gagne, E. J. Hopfinger, and R. A. Antonia, J. Fluid Mech. **140**, 63 (1984).
[5]R. A. Antonia, B. R. Satyprkash, and A. K. Hussain, Phys. Fluids **25**, 29 (1982).
[6]See, e.g., *Chaos*, edited by Hao Bai-Lin (World Scientific, Singapore, 1984).
[7]H. G. Schuster, *Deterministic Chaos* (Physik, Berlin, 1984).
[8]P. Tong, W. I. Goldburg, C. K. Chan, and A. Sirivat, Phys. Rev. A **37**, 2125 (1988).
[9]W. I. Goldburg and P. Tong, in *Fritz Haber International Symposium: Chaos and Related Nonlinear Phenomena* (Plenum, New York, in press).
[10]P. J. Bourke, J. Butterworth, L. E. Drain, P. A. Eglestaff, A. J. Hughes, P. Hutchinson, D. A. Jackson, E. Jakeman, B. Moss, J. O'Shaughnessy, E. R. Pike, and P. Schofield, J. Phys. A Gen. Phys. **3**, 216 (1970).
[11]B. J. Berne and R. Pecora, *Dynamic Light Scattering* (Wiley, New York, 1976).
[12]L. E. Drain, *The Laser Doppler Technique* (Wiley, New York, 1980).
[13]F. Durst, A. Melling, and J. H. Whitelaw, *Principles and Practice of Laser-Doppler Anemometry* (Academic, New York, 1981), 2nd ed.
[14]A. V. Smolyakov and V. M. Tkachenko, *The Measurement of Turbulent Fluctuations*, English edition (Springer, Berlin, 1983).
[15]J. L. Lumley, Phys. Fluids **8**, 1056 (1965).
[16]U. Frisch and G. Parisi, in *Turbulence and Predictability in Geophysical Fluid Dynamics and Climate Dynamics*, edited by M. Ghil, R. Benzi, and G. Parisi (North-Holland, New York, 1985), p. 84.
[17]T. C. Halsey, H. J. Mogens, L. P. Kadanoff, I. Procaccia, and B. I. Shraiman, Phys. Rev. A **33**, 1141 (1986).
[18]R. Benzi, G. Paladin, G. Parisi, and A. Vulpiani, J. Phys. A Gen. Phys. **17**, 3521 (1984).
[19]S. Corrsin, in *Handbuch der Physik*, edited by S. Flugge and C. Trusdell (Springer, Berlin, 1963), Vol. 8, part 2, p. 524.
[20]J. L. Lumley, Trans. ASME Ser. D, J. Basic Eng. **86**, 218 (1964).
[21]D. J. Tritton, *Physical Fluid Dynamics* (Van Nostrand Reinhold, New York, 1977).
[22]A. Onuki, Phys. Lett. A **127**, 143 (1988).
[23]A. Ralston, *A First Course in Numerical Analysis* (McGraw-Hill, New York, 1965).
[24]R. H. Kraichnan (private communication, 1987).
[25]N. A. Clark, H. J. Lunacek, and G. B. Benedek, Am. J. Phys. **38**, 575 (1970).
[26]P. Tong and W. I. Goldburg, Phys. Lett. A **127**, 147 (1988).